Simultaneous Block Copolymer and Magnetic Nanoparticle Assembly in Nanocomposite Films

Chen Xu,[†,||] Kohji Ohno,[‡] Vincent Ladmiral,[‡,⊥] Daniel E. Milkie,[§] James M. Kikkawa,[§] and Russell J. Composto*[,†]

Department of Materials Science and Engineering and Laboratory for Research on the Structure of Matter, University of Pennsylvania, Philadelphia, Pennsylvania 19104-6272; Institute for Chemical Research, Kyoto University, Uji, Kyoto 611-0011, Japan; and Department of Physics & Astronomy, University of Pennsylvania, Philadelphia, Pennsylvania 19104-6317

Received October 5, 2008; Revised Manuscript Received December 30, 2008

ABSTRACT: We investigate self-assembly of nanocomposite films composed of lamellar-forming poly(styrene-*b*-methyl methacrylate) (PS-*b*-PMMA) and PMMA-grafted magnetite (Fe_3O_4) nanoparticles (NPs). The Fe_3O_4 NPs are grafted with PMMA brushes with molecular weights ranging from 2700 to 35 700 g/mol. For the NP with the lowest molecular weight brush, the morphology of the nanocomposite film depends on the NP concentration (ϕ_{NP}). At low ϕ_{NP}, the block copolymer self-assembles into mixed morphology of perpendicular lamellae (⊥Lam) and parallel lamellae (||Lam), and the ⊥Lam are stabilized by individual NPs or small NP aggregates. The NPs can also retard the dynamics of self-assembly of block copolymer films. At high ϕ_{NP}, NPs form small aggregates which inhibit the formation of a lamellar structure. As the molecular weight of the PMMA brush increases to 13 300 or 35 700 g/mol, the Fe_3O_4 NPs form aggregates in the as-cast nanocomposite films, and this behavior is attributed to aggregation of NPs in the solution state. Since the size of NP aggregates is larger than the copolymer domain size, the block copolymer has to self-assemble around these aggregates. The magnetic properties of these nanocomposite films are characterized, and typical superparamagnetic behavior is observed.

Introduction

Although polymer nanocomposites (PNCs) are already found in numerous commercial products (e.g., tires), the incorporation of functional nanoparticles (NPs) having unique electric, optical, catalytic, and magnetic properties will provide future opportunities in technologies such as solar cells, photonic bandgap materials, and high-density magnetic storage devices.[1−3] To capitalize on these properties, NPs must be assembled or arranged in a controlled fashion with nanoscale precision and selectivity. For this reason, block copolymers are attractive as the continuous phase in PNCs because they self-assemble into ordered nanostructures that can be used to guide and control the location of NPs in selected domains.[4−11] Recent studies have incorporated functional NPs into block copolymers via an ex situ approach where preformed NPs are integrated into the nanostructure by cooperative self-organization.[12−19] For example, CdSe NPs were selectively deposited into templates of block copolymer poly(styrene-*b*-methyl methacrylate) (PS-*b*-PMMA) to produce a PNC that was photoluminescent.[20,21] Recently, magnetic NPs assembled in block copolymers has gained attention as a method to fabricate hybrid materials for applications such as high-density magnetic storage devices.[13,22−26] For example, Darling et al. deposited magnetic FePt NPs onto a film of PS-*b*-PMMA.[22] Magnetic NPs have also been incorporated into block copolymer films. Park et al. have assembled maghemite (γ-Fe_2O_3) NPs in poly(styrene-*b*-isoprene) (PS-*b*-PI).[25,26] By adding the γ-Fe_2O_3 NPs, a phase transition from hexagonal cylinders to body-centered cubic was observed as well as macrophase separation of NP-rich regions. Also, Lauter-Pasyuk et al. added magnetite (Fe_3O_4) NPs to PS-*b*-PBMA films to produce a mixed morphology of perpendicular and parallel lamellae on the surface, although the NP location was unknown.[23,24]

The NP characteristics, including size and surface functionality, can influence the self-assembly and ultimate structure of PNCs. For example, Bockstaller et al. demonstrated that, by tuning the NP diameter (d) relative to the lamellar period (L), NPs can be localized either in the middle of a domain ($d/L \sim 0.26$) or at the interface ($d/L \sim 0.06$) of a lamellar poly(styrene-*b*-ethylene propylene) (PS-*b*-PEP).[27] These results are supported by an entropy-based model by Balazs and co-workers,[28,29] who predicted that small particles satisfying $d/L < 0.2$ locate at the intermaterial dividing surface. However, later studies by Bockstaller et al. and Chiu et al. showed that small NPs can display a homogeneous or broad distribution within the preferred copolymer domain.[30,31] These contradictory results can be attributed to differing NP characteristics such as size, type, and surface functionality of NPs. Recently, Matsen et al. proposed an improved SCFT to better predict the distribution of NPs in a lamellar-forming diblock copolymer.[32] They found that small NPs have broader distributions but no particular preference for the interface. In their model, particle−polymer interactions are found to impact the location of NPs; i.e., neutral particles partition to the interface whereas particles attracted to one of the domains prefer to localize at the center of that domain. By varying the brush type, grafting density, and molecular weight, Kramer and co-workers were able to control the location of polymer-grafted Au NPs in poly(styrene-*b*-2-vinylprindine) (PS-*b*-P2VP) as well as the dimensions and morphology of the ordered block copolymer nanostructures.[31,33−36] For instance, beyond a critical concentration, Au NPs induced a phase transition of PS-*b*-P2VP from a lamellar to spherical morphology.[34] NPs also stabilize the energetically unfavorable grain boundaries or defects in block copolymers. Recently, Bockstaller et al. stabilized high-energy grain boundaries in lamellar block

* Corresponding author: phone (215) 898-4451, fax (215) 573-2128, e-mail composto@seas.upenn.edu.
† Department of Materials Science and Engineering and Laboratory for Research on the Structure of Matter, University of Pennsylvania.
‡ Kyoto University.
§ Department of Physics & Astronomy, University of Pennsylvania.
|| Present address: Arkema Inc., 900 First Avenue, King of Prussia, PA 19406.
⊥ Present address: Key Centre for Polymers & Colloids, School of Chemistry, University of Sydney, NSW 2006, Australia.

10.1021/ma8022266 CCC: $40.75
Published on Web 02/03/2009

copolymer films by selectively swelling the boundaries with aggregates of PS-grafted Au NPs.[37] In addition to changing the thermodynamic behavior and morphology, the addition of NPs also influences the dynamics of self-assembly of the copolymer. In a lamellar PS-*b*-PMMA film, Deshmukh et al. reported that Ag NPs slow down the surface transition from perpendicular to parallel lamellae.[38] This slowing down was attributed to the relocation of the surface-segregated Ag NPs, located in the PMMA domains, which must migrate below the surface to allow surface to become covered with PS lamellae (i.e., parallel lamellae at surface). Because few studies of the dynamics of self-assembly of PNCs are available, the mechanism of slowing down is not entirely understood.

The present paper describes the self-assembly of nanocomposite films of lamellar-forming PS-*b*-PMMA containing magnetite (Fe_3O_4) NPs which are grafted with PMMA brushes having molecular weights 2700, 13 300, and 35 700 g/mol. For the shortest brush at low concentrations ($\phi_{NP} = 1$ and 4 wt %), the block copolymer initially assembles into perpendicular lamellae (⊥Lam) at the surface, which eventually converts to parallel lamellae (||Lam). This behavior is qualitatively similar but much slower than rearrangements found in neat PS-*b*-PMMA systems. At 1 wt %, the NPs are mainly isolated and locate at the interface between domains, whereas at 4 wt % the NPs aggregate but remain confined within the PMMA domain ($L/2 = 18$ nm). At 4 wt %, NPs are swept laterally to the grain boundary between ⊥Lam and ||Lam, resulting in long-lived ⊥Lam at the surface. At $\phi_{NP} = 10$ wt %, NPs form aggregates whose size is comparable to the PMMA domain size. Although the ⊥Lam covers the entire surface at long times (192 h), the bulk region shows a disordered, possibly bicontinuous, morphology of PS-*b*-PMMA. As brush length increases, the solubility of NPs in solution decreases, resulting in aggregates in the as-cast PNC films, and this behavior is attributed to aggregation of NPs in the solution state, prior to spin-casting. For the 13 300 case, NP aggregates are slightly larger than the PMMA domain size and tend to locate at grain boundaries, resulting in stabilized ⊥Lam morphology at the surface even after 240 h. However, for the 35 700 brush, aggregates up to 164 nm form, disrupt the ||Lam, and become encapsulated by onion-type layers of PS-*b*-PMMA. Since the size of NP aggregates is larger than the copolymer domain size, the block copolymer has to self-assemble around these aggregates. The blocking temperature, which represents the energy barrier for magnetic relaxation, is found to be the same for well -dispersed and aggregated PNCs, suggesting that a polymer brush of 35 700 g/mol provides sufficient magnetic isolation between NPs.

Experimental Section

Materials and Methods. Poly(styrene-*b*-methyl methacrylate) (PS-*b*-PMMA) with a polydispersity of 1.08 was purchased from Polymer Source, Inc. The molecular weights (M_n) and the volume fractions of the PS and PMMA blocks are 38 000 and 36 800 g/mol and 0.53 and 0.47, respectively. The magnetite NPs (~5 nm) were synthesized and characterized following the methods described by Sun et al.[39] The NPs were then modified by grafting PMMA chains onto the surface via surface-initiated atom transfer radical polymerization (ATRP), and the details of this surface-initiated ATRP method have been well described in one of our previous papers.[40] To determine the molecular weight and polydispersity of the grafted polymer brush, PMMA chains were cleaved from the NP surface as follows: the PMMA-grafted magnetite NPs and tetraoctylammonium bromide as a phase transfer catalyst were dissolved in toluene, to which a 10% HF aqueous solution was added. Because the initiation sites on the NP are formed by a silane coupling agent, the Si−O bond between the PMMA brush and iron oxide surface is broken by the HF. The cleaved polymer in the organic layer was isolated and then subjected to gel permeation chromatography (GPC). Three PMMA brushes with molecular weights (M_n) of 2.7, 13.3, and 35.7 kg/mol were prepared, and the corresponding PMMA-grafted magnetite NPs are denoted as Fe_3O_4-2.7K, Fe_3O_4-13.3K, and Fe_3O_4-35.7K, respectively. The polydispersity indexes of these brushes determined by GPC are 1.22, 1.10, and 1.15, respectively. The grafting density (Σ) was calculated to be 0.73 ± 0.02 chains/nm^2 for all three NPs based on the weight fraction of PMMA chains (determined by thermal gravimetric analysis), the surface area of NPs, and densities of PMMA and magnetite.

To prepare the PNC films, the block copolymer and NPs (7 wt %) are mixed with toluene. The weight fraction of NPs in the PNC ranges from 1 to 16 wt %. Nanocomposite films were prepared by spin-casting the block copolymer−nanoparticle solution onto piranha-cleaned silicon substrates. The films were dried in a vacuum oven at room temperature for 1 day, and their thicknesses were about 500 nm. The films were then annealed under vacuum at 185 °C for 2−240 h.

Characterization. Atomic force microscopy (AFM, PicoPlus, Agilent Technologies, Inc.) was used to characterize the surface morphology of the PNC films. The microscope was operated in the acoustic AC (AAC) mode. Silicon cantilevers (Nanosensors, Inc.) with a nominal spring constant of 48 N/m and tip radius of less than 10 nm were used. The resonance frequency of the cantilevers is about 190 kHz. Picoscan 5.3.3 (Agilent Technologies, Inc.) and SPIP (Image Metrology, Inc.) were used for image analysis. Transmission electron microscopy (TEM, JEOL 2010) operated at 80 kV was used to image the block copolymer morphology and NP location within the films. To prepare TEM cross section, nanocomposite films were coated with an epoxy layer and then immersed into liquid N_2 to delaminate the bilayers of epoxy/nanocomposite film from the silicon substrates. The epoxy-supported nanocomposite films were microtomed into ~50 nm slices with a diamond knife at room temperature. The microtomed sections were then transferred onto holey carbon-coated copper grids. Magnetization of the PNC films was measured in a Quantum Design Superconducting Quantum Interference Device (SQUID) magnetometer. In particular, the temperature dependence of zero-field-cooled (ZFC) and field-cooled (FC) magnetic moment and $M-H$ magnetization curves were measured.

Results and Discussion

Morphology Evolution of PS-*b*-PMMA/Fe_3O_4-2.7K (ϕ_{NP} = 1 wt %) Films. In this section, we investigate the location of Fe_3O_4-2.7K NPs in PNC films as well as the effect of these NPs on the morphology and evolution of block copolymer self-assembly. Figure 1 shows the surface and internal morphologies of PS-*b*-PMMA/Fe_3O_4-2.7K (1 wt %) films after annealing at 185 °C for 2 h (a, b), 8 h (c, d), and 24 h (e, f). After 2 h, the surface is covered by perpendicular lamellae (⊥Lam) that appear as alternating stripes (also called "fingerprint" features) in the AFM height image (Figure 1a). By taking a 2D fast Fourier transform (FFT) of the AFM image (inset in Figure 1a), the lamellar spacing of the ⊥Lam at the film surface is 41 nm. Using $L = 0.47N^{0.65}$, the lamellar period of the bulk morphology is 34.2 nm.[41] In this paper, L is determined to be 37 nm as discussed below.[38] The light (higher) stripes correspond to PMMA lamellae, whereas the dark (lower) stripes are the PS lamellae. The height difference between the PMMA and PS lamellae is ~1 nm, consistent with the literature.[38,42] Because of favorable interactions, PMMA chains prefer the oxide layer on silicon and thus form a parallel lamellar (||Lam) monolayer on the substrate, as shown in Figure 1b. After 2 h, Figure 1b captures the propagation of the ||Lam from the substrate to about the middle of the film. In the TEM images, the PMMA and PS domains are light and dark, respectively. The NPs are preferentially located in the PMMA domains. Further discussion of NP location is given below. Although the ⊥Lam are observed at the film surface by AFM, they can hardly be discerned in the TEM image (Figure 1b), suggesting that only very short-

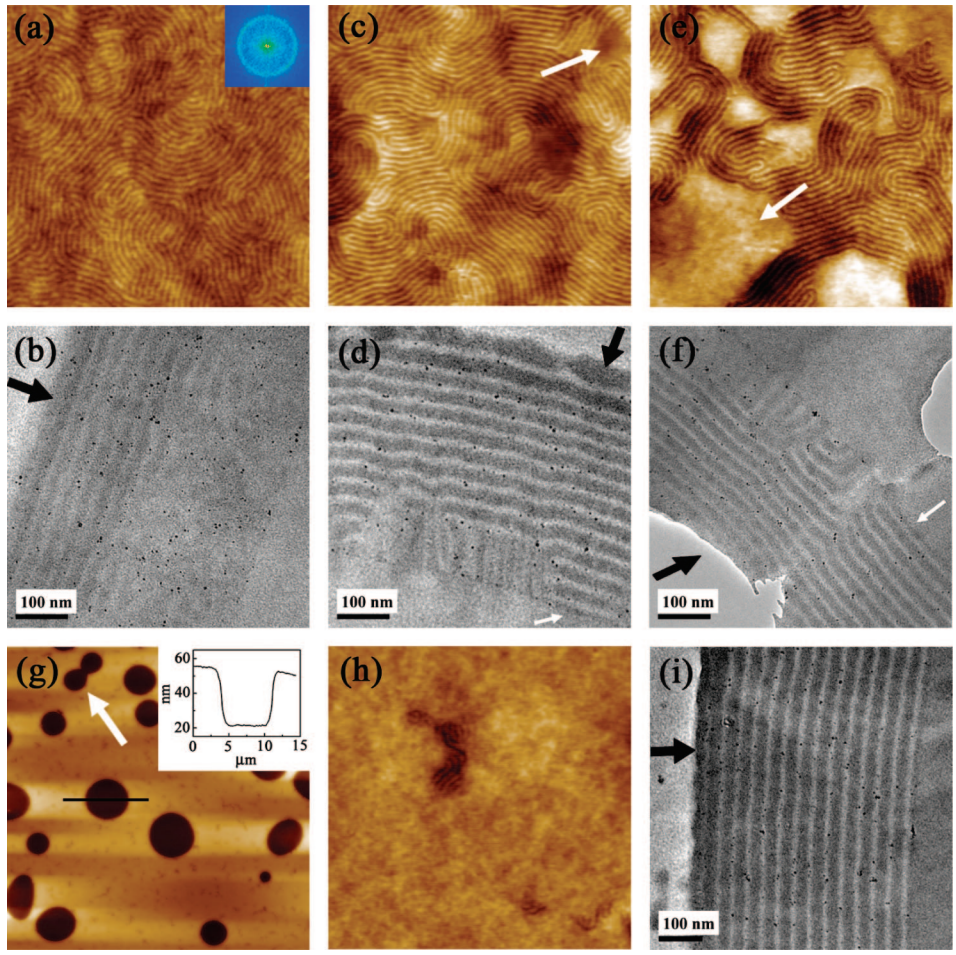

Figure 1. AFM height and cross-sectional TEM images of PS-*b*-PMMA/Fe_3O_4-2.7K (1 wt %) films after annealing at 185 °C for 2 h (a, b), 8 h (c, d), and 24 h (e, f). Inset in (a) is a 2D FFT of the image. Black arrows in the TEM images indicate the film/substrate interface, whereas white arrows in (c, d, e, f) indicate the ||Lam on the surface. AFM height (g, h) and cross-sectional TEM (i) images of films after 240 h are also shown. The inset in (g) is a cross-sectional line profile across the hole (black line) shown in the parent image. The size of AFM images (a, c, e, h) is 2 × 2 μm^2, and the height scale is $\Delta z = 0-8$ nm. The AFM image size for (g) is 50 × 50 μm^2, and the height scale is $\Delta z = 0-80$ nm.

range ⊥Lam form at the surface. Thus, after 2 h or the early stage, PS-*b*-PMMA self-assembles into ||Lam near the silicon substrate and ⊥Lam near the surface, whereas the NPs are evenly dispersed throughout the film.

After annealing for 8 h, smooth patches corresponding to ||Lam appear on the surface, as indicated by the white arrow in Figure 1c. In the ||Lam regions, the PS block, which has the lower surface energy, is exposed on the surface.[38] This structure is confirmed by the AFM phase images (not shown) and cross-sectional TEM images as shown in Figure 1d. Thus, at this intermediate stage the surface displays a mixed morphology of ⊥Lam and ||Lam, similar to neat PS-*b*-PMMA films or PS-*b*-PMMA films containing NPs.[38,43] Compared to the image after 2 h (Figure 1b), the block copolymer morphology is more ordered after 8 h (Figure 1d). Note that the ||Lam has 10 complete periods and in some regions has propagated to the surface (indicated by the white arrow), resulting in a mixture of ||Lam and ⊥Lam (Figure 1d). In the ||Lam regions, the PS lamellar domains (dark) are at the surface (white arrow in Figure 1d).

After 24 h (Figure 1e), the area fraction of the ||Lam domains on the surface has increased compared to 8 h (Figure 1c). Namely, the PS-*b*-PMMA chains within the ⊥Lam regions near the surface reorganize and increase the area fraction of ||Lam at the surface in order to reduce the surface energy. Figure 1f shows a cross section of the mixed morphology of ⊥Lam and ||Lam in the near surface region. After both 8 and 24 h, the ⊥Lam penetrate three and half lamellar periods below the surface, as shown in parts d and f of Figure 1, respectively. This depth is determined by the film thickness and the relative ordering speed of the ⊥Lam and ||Lam. After 240 h, the surface is covered with holes of average diameter of 5.1 ± 1.5 μm. Hole formation, characteristic of ||Lam, is due to the incommensurability of the film thickness and the lamellar period; i.e., the film thickness is not equal to $(n + {}^1/_2)L$, where n is an integer.[44] The depth of these characteristic holes is equal to one lamellar period. Here, the depth of those holes is 37 nm, determined by the cross-sectional line profile analysis (inset in Figure 1g). As indicated by the arrow in Figure 1g, holes can merge to form larger holes. Although the surface is mainly covered by ||Lam after 240 h, careful inspection of Figure 1g shows very small regions of the ⊥Lam, which are better observed in Figure 1h (2 × 2 μm^2). Because the area fraction of ⊥Lam on the surface is so small, TEM images such as shown in Figure 1i show a nearly complete conversion to the ||Lam after 240 h. Relative to neat films, which achieve a complete ||Lam morphology after 24 h (discussed below), the addition of 1 wt % Fe_3O_4-2.7K NPs to PS-*b*-PMMA slows down the transition from ⊥Lam to ||Lam at the surface.

NP-Stabilized Defects in PS-*b*-PMMA/Fe_3O_4-2.7K (ϕ_{NP} = 4 wt %) Films. Figure 2 shows the AFM height images and cross-sectional TEM images of the surface and internal morphologies of PS-*b*-PMMA films containing 4 wt % of Fe_3O_4-2.7K. For the as-cast film, parts a and b of Figure 2 show that

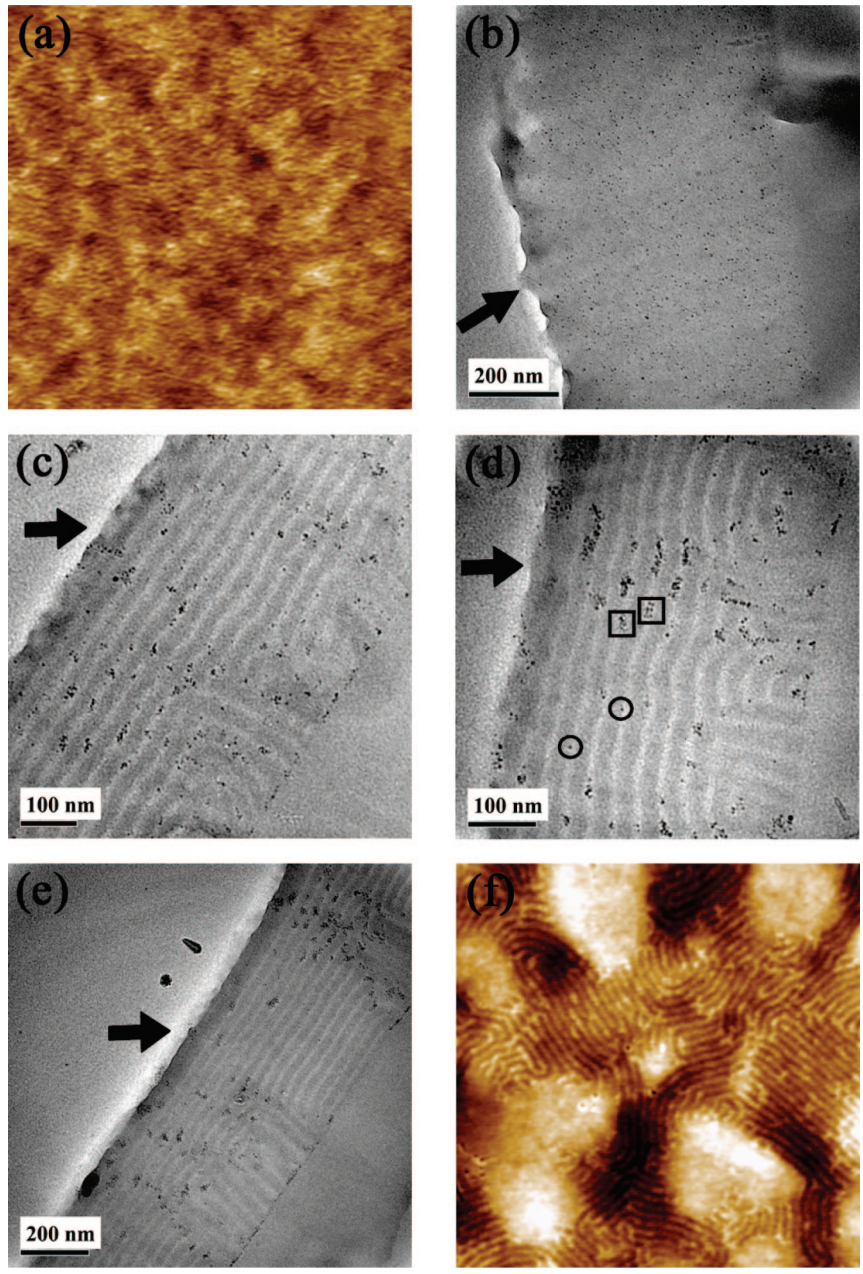

Figure 2. Surface and internal morphologies of PS-*b*-PMMA/Fe_3O_4-2.7K (4 wt %) films. AFM height (a) and cross-sectional TEM (b) images of as-cast nanocomposite films. Cross-sectional TEM images of nanocomposite films after annealing at 185 °C for 24 h (c), 96 h (d), and 240 h (e). The arrows in the TEM images indicate the film/substrate interface. AFM height image of nanocomposite films after annealing at 185 °C for 240 h (f). The size of AFM images (a, f) is $2 \times 2\ \mu m^2$, and the height scale is $\Delta z = 0-8$ nm.

the surface displays irregular features and the bulk morphology is disordered with a uniform dispersion of NPs, respectively. After annealing for 24−240 h (Figure 2c−e), the PS-*b*-PMMA in the films all display a similar morphology consisting of ||Lam near the substrate and a mixed ||Lam and ⊥Lam on the surface. However, unlike the individual NPs observed for 1 wt % NPs under all conditions, the initially uniform dispersion of 4 wt % NPs evolves into small aggregates upon annealing, as shown in Figure 2c−e.

Although NPs form aggregates upon annealing, these aggregates remain confined within the PMMA lamellar domains at all times. Initially (24 h), the aggregates contain ~5 NPs and are relatively uniformly dispersed as shown in Figure 2c; however, with longer annealing (96 h), aggregate size increases, ~10 NPs, and the lateral distribution becomes less uniform as shown in Figure 2d. This suggests that the NPs are mobile and can diffuse in the PMMA lamellae to form larger aggregates. In Figure 2d, the squares denote aggregates confined within the PMMA domains, whereas the circles denote individual NPs located mainly at the PS/PMMA interface. Here, although a few individual NPs are located more toward the center of the PMMA domain, most individual Fe_3O_4-2.7K NPs in PS-*b*-PMMA ($d/L = 0.15$) locate at the copolymer interface (e.g., NPs in Figures 1i and 2d). As discussed in the Introduction, the location of NPs depends on many parameters including particle size and their surface functionality. The improved Matsen's SCMF model could give nice predictions on NP location at low concentrations of NPs (<1%), whereas the present study is focused on the aggregation behavior of NPs confined to the lamellar phase of a diblock copolymer.[32] Thus, a comparison with the observed aggregation behavior is not possible. Moreover, the statistically small number of individual NPs prevents a definitive statement about the distribution of NPs except to note that a majority of particles are found at the

interface and a minority in the middle region. Confined by the PMMA lamellar domains, the Fe_3O_4-2.7K NPs aggregate within the lamellar plane and thus form 2-dimensional disk-shaped aggregate structure.

After annealing for 240 h, the NPs and aggregates further rearrange within the film. In particular, most NPs are now found in aggregates. Furthermore, these aggregates tend to locate at T-junction defects, where the ||Lam intersects the ⊥Lam, as shown in Figure 2e. This lateral partitioning results in large regions of the sample that contain ||Lam devoid of NPs (cf. Figure 2e). Because of chain stretching as well as an increase in interfacial area, T-junction defects or grain boundaries are energetically unfavorable and thus are thermodynamically unfavorable in neat block copolymers. Recent simulations by Duque et al. showed that T-junction grain boundaries can be stabilized by adding a homopolymer A to an A-*b*-B copolymer because the segregation of A can relieve chain stretching in the grain boundary region.[45] This prediction was supported by studies of poly(isoprene) added to poly(styrene-*b*-isoprene).[46] A similar study showed that homopolymer would concentrated in the corner regions (i.e., defects) of block copolymer films deposited on patterned substrates.[47] More recently, Bockstaller et al. provided direct evidence for the stabilization of energetically unfavorable gain boundaries by selectively swelling the defects with aggregates of PS-grafted Au NPs.[37] In a similar manner, the Fe_3O_4-2.7K NPs investigated in this study selectively locate in the T-junction defects to relax the mechanical stresses due to the chain stretching and therefore stabilize the defects. As a result, the thermodynamically unfavorable ⊥Lam are effectively pinned. Figure 2e shows a typical cross section consisting of ||Lam that span the entire film alternating with mixed morphology of ||Lam near the substrate and ⊥Lam near the surface. The lateral separation between the stabilized ⊥Lam varies from ∼200 to ∼1000 nm. Figure 2f reveals the surface morphology of a PS-*b*-PMMA/Fe_3O_4-2.7K (4 wt %) film after 240 h. The smooth patches correspond to ||Lam with a top PS domain, whereas the alternating stripes represent the ⊥Lam stabilized by the Fe_3O_4-2.7K NPs. Thus, the addition of 4 wt % Fe_3O_4-2.7K NPs to PS-*b*-PMMA provides a novel route for producing a long-lived surface displaying ⊥Lam domains with a coverage that can be tuned by NP concentration.

Effect of NP Concentration on Ordering Dynamics in PS-*b*-PMMA/Fe_3O_4-2.7K Films. The dynamics of the morphology transition from ⊥Lam to ||Lam can be quantified by analyzing AFM images. To determine the area fraction of ⊥Lam at a given time, large scan size images (up to 20 × 20 μm^2) were acquired over different areas of the same and duplicate samples. Figure 3 shows the area fraction of ⊥Lam on the surface as a function of annealing time for $\phi_{NP} = 0$, 1, and 4 wt %. After 2 h, the surface is entirely covered by ⊥Lam for all ϕ_{NP}, indicating that the propagation of ||Lam domains from the substrate has not yet reached the surface region. The area fraction of ⊥Lam decreases upon further annealing. For neat PS-*b*-PMMA films, the area fraction of ⊥Lam decreases rapidly with annealing time, and the surface is completely converted to ||Lam after 24 h. However, the morphology transition from ⊥Lam to ||Lam slows down with the addition of Fe_3O_4-2.7K NPs, and this slowing down becomes stronger as ϕ_{NP} increases. At 1 wt %, the area fraction of ⊥Lam decreases rapidly to 33.5% after 24 h and then more slowly to 4.5% after 240 h. Compared to the neat copolymer case, the existence of ⊥Lam in PS-*b*-PMMA/Fe_3O_4-2.7K (1 wt %) films after 240 h indicates that NP can stabilize the ⊥Lam. At 4 wt %, the transition from ⊥Lam to ||Lam is very slow, and the area fraction of ⊥Lam remaining near the surface after 240 h is 75.7%, significantly larger than that of the 1 wt % case. The slowing down of the morphology transition may, in part, result from an increase of the effective

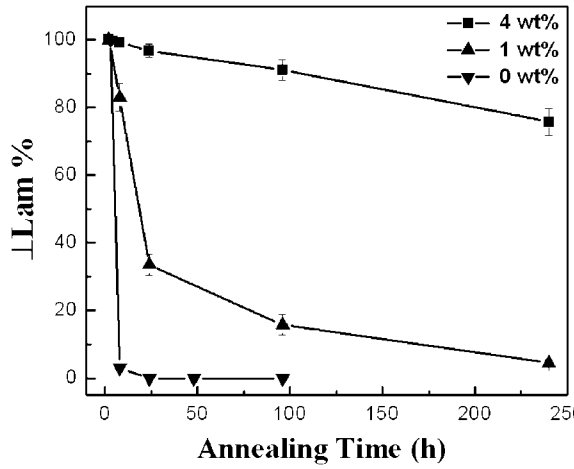

Figure 3. Area fraction of ⊥Lam on the surface as a function of annealing time for 0, 1, and 4 wt % Fe_3O_4-2.7K. The addition of NPs slows down the ⊥Lam to ||Lam transition and stabilizes the ⊥Lam morphology due to segregation NPs and aggregate formation at grain boundaries.

block copolymer viscosity upon adding NPs. Recent studies show that NPs can slow down the phase separation of polymer blends and even stabilize bicontinuous structures at high concentrations.[48] In the present study, the stabilization of ⊥Lam is mainly achieved by the segregation of PMMA-grafted NPs to the T-junction defects. Recently, Deshmukh et al. reported that in situ prepared Ag NPs can also slow down the transition from ⊥Lam to ||Lam of PS-*b*-PMMA.[38] This surface transition requires the redistribution of surface-segregated NPs located in the ⊥Lam to diffuse below the surface; at 5 wt % Ag NP, the ⊥Lam morphology is pinned similar to the effect observed by adding 4 wt % Fe_3O_4-2.7K to PS-*b*-PMMA in the present study.[38]

Frustrated Ordering of PS-*b*-PMMA/Fe_3O_4-2.7K (ϕ_{NP} = 10 wt %) Films. As discussed earlier, the addition of Fe_3O_4-2.7K NPs at $\phi_{NP} \leq 4$ wt % can slow down the transition from ⊥Lam to ||Lam and stabilize the ⊥Lam morphology. The surface and internal morphologies depend on ϕ_{NP}. Namely, at long times, ||Lam domains dominate the surface at 0 and 1 wt %, whereas ⊥Lam domains are long-lived at 4 wt %. In this section, we show that the addition of 10 wt % NPs frustrates block copolymer self-assembly and results in aggregates on the size scale of the PMMA domains, ∼20 nm.

Figure 4 shows the AFM height images and cross-sectional TEM images of PS-*b*-PMMA/Fe_3O_4-2.7K (10 wt %) films. Before annealing, the surface shows random, irregular features as shown in Figure 4a. The NPs are uniformly dispersed in the block copolymer film, and the morphology of PS-*b*-PMMA is disordered (Figure 4b). After annealing for 24 h, Figure 4c shows that ⊥Lam begin to appear at the surface with very short-range order, ∼150 nm lateral size. This short-range order is in contrast to the longer range fingerprint pattern observed at ϕ_{NP} = 1 wt % (Figure 1a) and 4 wt % (not shown). More strikingly, Figure 4d shows that the PS-*b*-PMMA is unable to self-assemble into a lamellar structure after 24 h, in contrast to the $\phi_{NP} = 4$ wt % case (Figure 2c). Simultaneously, the Fe_3O_4-2.7K NPs form aggregates of average size 22 nm. These aggregates are uniformly dispersed throughout the bulk and apparently prevent PS-*b*-PMMA chains from forming a lamellar structure. Rather, the PMMA block (light region in Figure 4d) encapsulates the aggregates, suggesting that the block copolymer assembles around the aggregates. After a longer annealing (192 h), the surface shows slightly better ordering of lamellae (Figure 4e). After they form, these aggregates are quite stable and neither

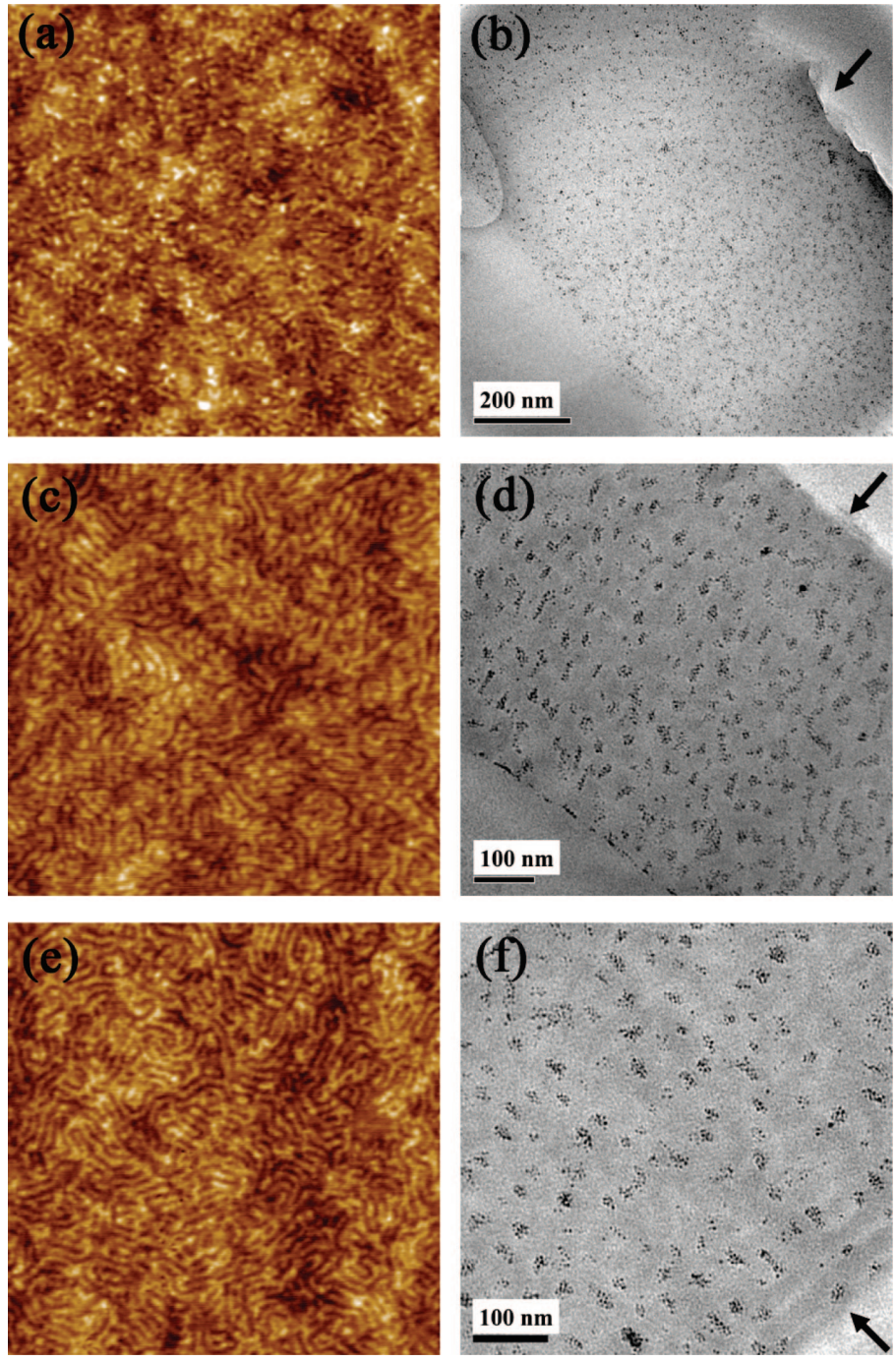

Figure 4. Surface and internal morphologies of PS-*b*-PMMA/Fe_3O_4-2.7K (10 wt %) films. AFM height images and cross-sectional TEM images of as-cast films (a, b) and films after annealing at 185 °C for 24 h (c, d) and 192 h (e, f). The size of all AFM images (a, c, e) is 2×2 μm^2, and the height scale is $\Delta z = 0-8$ nm for (a) and $\Delta z = 0-5$ nm for (c, e). Arrows in TEM images indicate the film/substrate interface.

grow nor redistribute upon further annealing, as shown in Figure 4f. The PS-*b*-PMMA remains randomly located around the aggregates in the bulk although two or three layers of ||Lam near the silicon substrate begin to appear as noted by the arrow in Figure 4f. Note that the PMMA domains (light) appear to form a continuous pathway, suggesting a bicontinuous structure may have been induced by the aggregates. By using NPs that segregate to the domain interface, Kim et al. observed the formation of bicontinuous structures in symmetric block copolymer.[36] Thus, our studies suggest an alternative pathway to create nanoscale interconnected domains.

Effect of Brush Molecular Weight on NP Aggregation. In as-cast PS-*b*-PMMA/Fe_3O_4-13.3K (4 wt %) films, we previously observed that these NPs are found as both isolated single NPs and in large aggregates (~37.6 nm) as shown in Figure 5a.[49] After annealing at 185 °C for 96 h, the film surface consists of a mixed morphology of ⊥Lam and ||Lam, as shown in the AFM height (Figure 5b) and phase (Figure 5c) images. In the ⊥Lam regions, circular features wider than the individual lamellae are observed as denoted by the arrow in Figure 5b. In Figure 5c, these features have the same phase contrast as the PMMA lamellar stripes (light stripes), suggesting that these circular regions are PMMA-grafted Fe_3O_4 aggregates near the surface. This identification is confirmed by a cross-sectional TEM image (inset in Figure 5b) showing Fe_3O_4-13.3K NP aggregates located near the surface. Figure 5d shows the internal structure of the nanocomposite film after annealing for 96 h. The mixed morphology of ⊥Lam and ||Lam is observed. The Fe_3O_4-13.3K

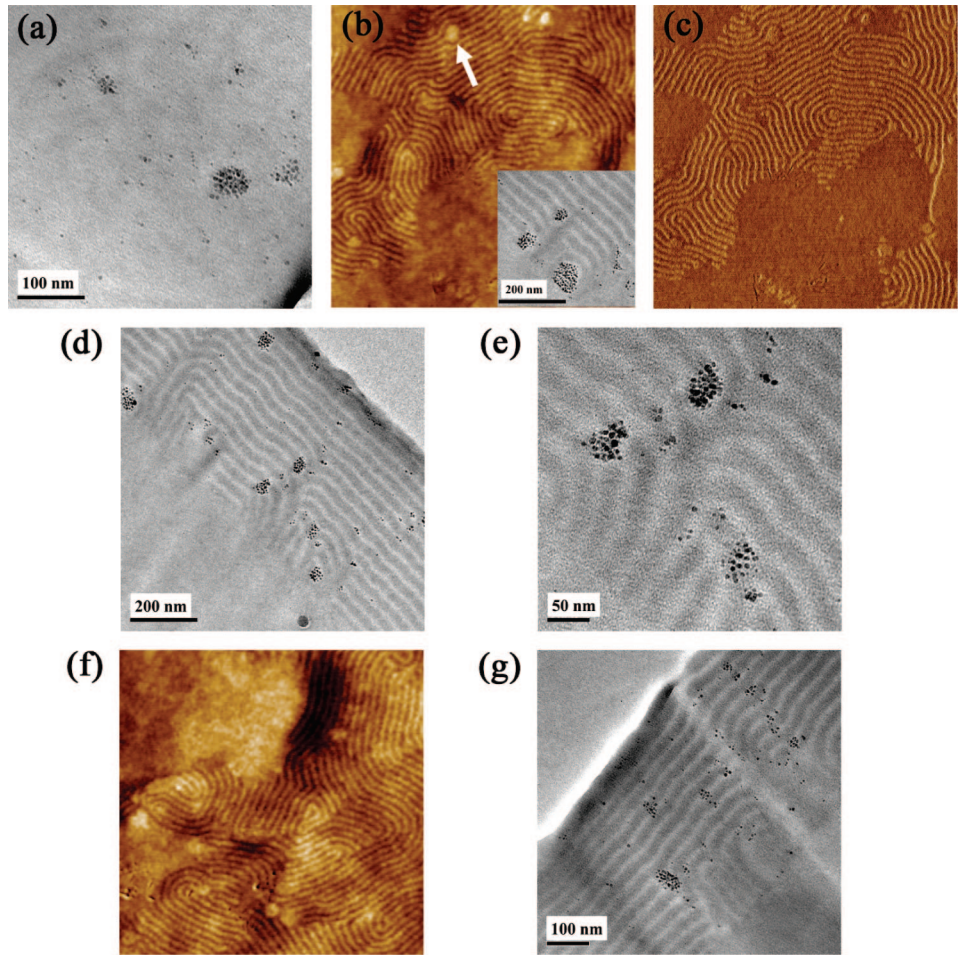

Figure 5. (a) Cross-sectional TEM image of as-cast PS-*b*-PMMA/Fe_3O_4-13.3K (4 wt %) film. AFM height (b), phase (c), and cross-sectional TEM (d, e) images of PS-*b*-PMMA/Fe_3O_4-13.3K (4 wt %) film after annealing at 185 °C for 96 h. Inset in (b) is a cross-sectional TEM image showing NP aggregates at the surface. AFM height (f) and cross-sectional TEM (g) images of PS-*b*-PMMA/Fe_3O_4-13.3K (4 wt %) film after annealing at 185 °C for 240 h.

NPs remain as individual NPs and aggregates in the block copolymer film, suggesting that the NP aggregates formed during casting remain upon annealing. Because the aggregates are usually larger than the PMMA lamellar domain (~18 nm), these aggregates force the lamellar structure to terminate and become encapsulated by the PMMA domains as shown in Figure 5e, a high-magnification TEM image. As observed in Fe_3O_4-2.7K case at 4 wt %, the aggregates tend to locate at the grain boundary between ⊥Lam and ||Lam and stabilize the ⊥Lam at the surface. After 240 h, the surface morphology and internal structure remain very similar to that observed at 96 h as shown in parts f and g of Figure 5, respectively.

Upon increasing the brush molecular weight from 13 300 to 35 700 g/mol, the NP aggregation in PS-*b*-PMMA films increases. In contrast to Fe_3O_4-13.3K NPs, the Fe_3O_4-35.7K NPs are mainly found in aggregates in the as-cast films.[49] As ϕ_{NP} increases from 4 to 16 wt %, the average aggregate size increases from 42.7 to 164.0 nm.[49] After annealing at 185 °C for 240 h, Figure 6a shows that the surface morphology of a PS-*b*-PMMA/Fe_3O_4-35.7K (4 wt %) film displays a mixture of ⊥Lam and ||Lam. Quantitative analysis of several images yields a ||Lam area fraction and domain size of 29.8 ± 3.0% and ~300−1000 nm, respectively. Parts b and c of Figure 6 are representative cross-sectional TEM images with arrows denoting the surface. Similar to the Fe_3O_4-13.3K NP case, the aggregates are larger than the PMMA lamellar domains, resulting in a perturbed morphology with stabilized ⊥Lam. Figure 6d displays the surface morphology of a PS-*b*-PMMA/Fe_3O_4-35.7K (16 wt %) film after 240 h. In contrast to the ϕ_{NP} = 4 wt % case, the film surface is dominated by ⊥Lam. The ||Lam area fraction is only 2.5 ± 0.6%, and the domain size, which is rather monodisperse, is about 180 nm. For ϕ_{NP} = 16 wt %, Figure 6e,f shows the formation of large aggregates, about 30−50% of film thickness, which is much larger than the block copolymer period. As a result, the PS-*b*-PMMA has to assemble around the aggregates, with the PMMA domain on the inside, to produce an onionlike morphology. In these figures the arrows indicate the ||Lam, induced by confinement of the onionlike morphology adjacent to the surface.

Magnetic Properties of Block Copolymer Nanocomposites. Magnetite (Fe_3O_4) is a ferrimagnetic oxide of considerable interest because it exhibits a complex metal−insulator transition near 100 K (Verwey transition) and is also easily prepared in nanocrystalline form. Nanometer-sized magnetite is superparamagnetic.[50−54] Namely, NP magnetic moments are single-domain, pinned by anisotropy at low temperature, and thermally disordered above a characteristic blocking temperature, T_b.[55] Figure 7 shows the block copolymer nanocomposite films containing PMMA-grafted Fe_3O_4 NPs are indeed superparamagnetic. We obtained zero-field-cooled (ZFC), field-cooled (FC), and magnetization curves for block copolymer nanocomposite films having well-dispersed NPs as well as aggregates of NPs. For an as-cast PS-*b*-PMMA/Fe_3O_4-2.7K (10 wt %) film with a uniform dispersion of NPs (cf. Figure 4b), the ZFC and FC curves are presented in Figure 7a. Here T_b locates the

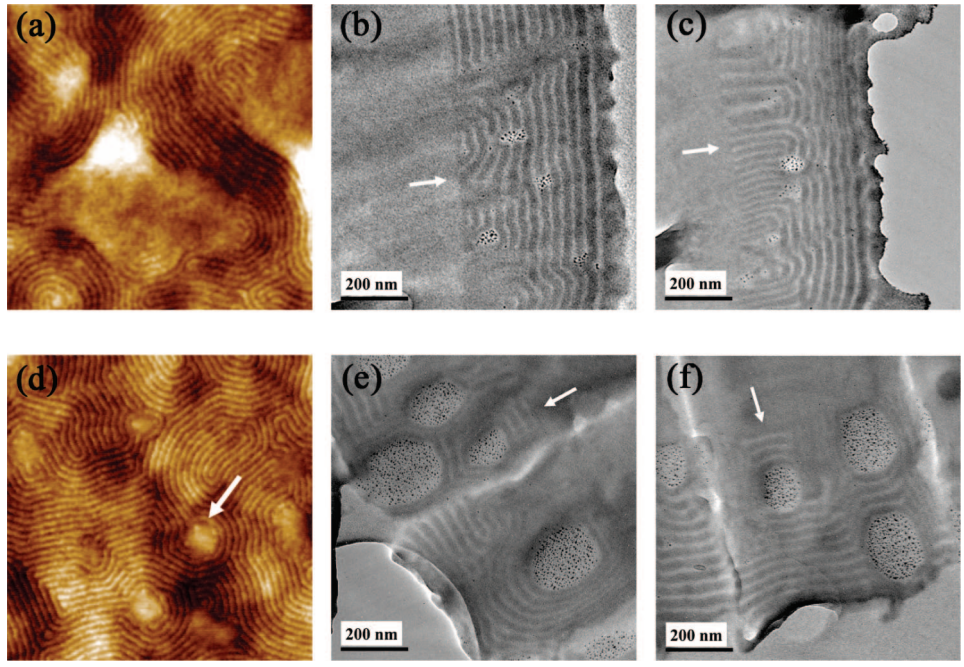

Figure 6. AFM height (a) and cross-sectional TEM images (b, c) of PS-*b*-PMMA/Fe_3O_4-35.7K (4 wt %) films after annealing at 185 °C for 240 h. AFM height (d) and cross-sectional TEM images (e, f) at $\phi_{NP} = 16$ wt % for the same annealing conditions. The dimensions of the AFM images are $2 \times 2\ \mu m^2$, and the height scale is $\Delta z = 0-8$ nm. Arrows in TEM images indicate the film/air interface.

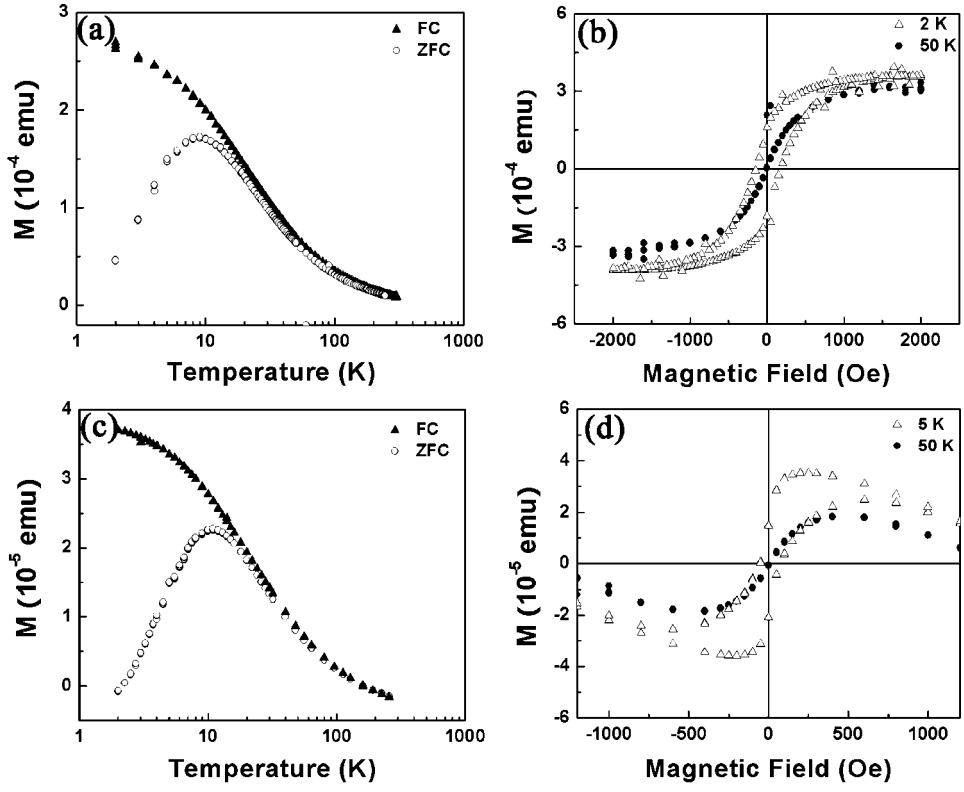

Figure 7. Magnetic properties of as-cast PS-*b*-PMMA/Fe_3O_4-2.7K (10 wt %) films: ZFC and FC curves at 100 Oe (a) and $M-H$ curves at 2 and 50 K (b). Magnetic properties of PS-*b*-PMMA/Fe_3O_4-35.7K (16 wt %) films after annealing at 185 °C for 240 h: ZFC and FC curves at 100 Oe (c) and $M-H$ curves at 5 and 50 K (d). Note: both (b) and (d) include diamagnetic contributions from the block copolymer matrix and sample holder. In the case of (d) these contributions are sufficient to produce a negative slope at high fields.

maximum magnetization on the ZFC curve and reflects the energy barrier for magnetic relaxation. For the PS-*b*-PMMA/Fe_3O_4-2.7K (10 wt %) film, T_b is ~9 K. Figure 7b shows the $M-H$ curves PS-*b*-PMMA/Fe_3O_4-2.7K (10 wt %) at 2 and 50 K. For $T < T_b$, the $M-H$ curve shows a distinct hysteresis with a coercivity of ~176 Oe, whereas for $T > T_b$, a reversible behavior is observed, consistent with a superparamagnetic response below and above the blocking temperature, respectively.

Estimation of T_b based on the bulk anisotropy constant and particle volume usually proceeds according to the Arrhenius relation $\tau = \tau_0 \exp(-KV/k_BT_b)$, where K is the anisotropy

constant, V is the NP volume, k_B is the Boltzmann constant, τ is the measurement time scale, and τ_0 is a characteristic attempt period of order 1 ns.[55] For Fe_3O_4 NP diameters of order 10 nm, the bulk anisotropy constant often underestimates T_b by an order of magnitude,[50,56,57] and the Arrhenius relation then empirically determines a correspondingly larger effective anisotropy, K_{eff}. The latter includes finite size effects, shape anisotropy, and chemical alteration of the surface layer, parameters which vary according to synthesis. Nevertheless, the values reported elsewhere universally suggest $T_b \sim 10^2$ K for $\sim$10 nm diameter Fe_3O_4,[50−54] an order of magnitude higher than our observation (9 K), which is in closer accord with bulk theoretical estimates for spherical particles.

One possibility is that this difference reflects the care taken in the present work to surround the NP with an isolating polymer brush. Many groups have studied the influence of long-range dipolar interactions on NP magnetic properties, which are seen to increase the anisotropy experimentally[57−59] and theoretically[60] and ultimately can give rise to spin glass[61] or, more recently, spin ice behavior.[62] Here, it is possible that the NPs retain more of their intrinsic magnetic character due to relatively small dipolar interactions. This hypothesis is at least consistent with our further observations. To control the separation between NPs, we selected one nanocomposite film with good dispersion of individual NPs, as previously discussed, and another with NPs mainly in large aggregates. On the basis of the morphology studies in this and another paper,[49] we chose to investigate the magnetic properties of PS-*b*-PMMA/Fe_3O_4-35.7K (16 wt %) annealed at 185 °C for 240 h. As shown in Figure 6e,f, this system has aggregates with a diameter of about 164 nm. Parts c and d of Figure 7 present the ZFC and FC curves and $M-H$ curves. The T_b is $\sim$11 K, nearly the same as the well-dispersed Fe_3O_4-2.7K shown in Figure 7a. This observation suggests that a PMMA brush of molecular weight 35.7K separates Fe_3O_4 NPs enough to reduce the dipolar interaction, even when the NPs form aggregates. Hence, this composite may be able to obtain high particle densities without altering the NP magnetic properties. For the PS-*b*-PMMA/Fe_3O_4-35.7K system, the $M-H$ behavior shown in Figure 7d is qualitatively similar to the PS-*b*-PMMA/Fe_3O_4-2.7K system. Namely, below T_b, a hysteresis is observed with a coercivity of $\sim$60 Oe, whereas above T_b the response reflects superparamagnetic behavior.

Conclusions

In conclusion, we investigate the self-assembly process for nanocomposite films of lamellar-forming PS-*b*-PMMA and PMMA-grafted Fe_3O_4 NPs. At fixed grafting density, the Fe_3O_4 NPs are grafted with PMMA brushes having molecular weights of 2700, 13 300, and 35 700 g/mol. For the shortest PMMA brush, the morphology of nanocomposite films goes from dispersed to aggregated upon increasing NP concentration, ϕ_{NP}. For $\phi_{NP} \leq 4$ wt %, the PS-*b*-PMMA morphology at the surface evolves from ⊥Lam to a mixture of ⊥Lam and ||Lam. For $\phi_{NP} = 1$ and 4 wt %, the transition from ⊥Lam to ||Lam is slowed by the segregation of individual NP and small aggregates to grain boundaries, respectively. At $\phi_{NP} = 10$ wt %, NPs form small aggregates which frustrate the assembly of a lamellar structure. Upon increasing brush molecular weight, the Fe_3O_4 NPs are driven into large aggregates, relative to domain size, that appear in the as-cast films, and as a result, the block copolymer assembles into onionlike rings around these aggregates. The blocking temperatures of the nanocomposite films having well-dispersed and aggregated NPs are similar, suggesting that a 35.7K brush length is sufficient to prevent magnetic dipolar coupling between neighboring NPs.

Acknowledgment. This work was financially supported by grants from NSF/MRSEC (DMR05-20020) (R.J.C., J.M.K.), NSF/Polymer Program (DMR 05-49307) (R.J.C.), and NSF/NSEC (DMR04-25780) (R.J.C.).

References and Notes

(1) Bockstaller, M. R.; Mickiewicz, R. A.; Thomas, E. L. *Adv. Mater.* **2005**, *17* (11), 1331–1349.
(2) Lazzari, M.; Lopez-Quintela, M. A. *Adv. Mater.* **2003**, *15* (19), 1583–1594.
(3) Burda, C.; Chen, X. B.; Narayanan, R.; El-Sayed, M. A. *Chem. Rev.* **2005**, *105* (4), 1025–1102.
(4) Aizawa, M.; Buriak, J. M. *J. Am. Chem. Soc.* **2005**, *127* (25), 8932–8933.
(5) Aizawa, M.; Buriak, J. M. *J. Am. Chem. Soc.* **2006**, *128* (17), 5877–5886.
(6) Bates, F. S.; Fredrickson, G. H. *Annu. Rev. Phys. Chem.* **1990**, *41*, 525–557.
(7) Boontongkong, Y.; Cohen, R. E. *Macromolecules* **2002**, *35* (9), 3647–3652.
(8) Haryono, A.; Binder, W. H. *Small* **2006**, *2* (5), 600–611.
(9) He, J. B.; Tangirala, R.; Emrick, T.; Russell, T. P.; Boker, A.; Li, X. F.; Wang, J. *Adv. Mater.* **2007**, *19* (3), 381–385.
(10) Kashem, M. M. A.; Perlich, J.; Schulz, L.; Roth, S. V.; Petry, W.; Muller-Buschbaum, P. *Macromolecules* **2007**, *40* (14), 5075–5083.
(11) Lopes, W. A.; Jaeger, H. M. *Nature (London)* **2001**, *414* (6865), 735–738.
(12) Adachi, M.; Okumura, A.; Sivaniah, E.; Hashimoto, T. *Macromolecules* **2006**, *39* (21), 7352–7357.
(13) Ahmed, S. R.; Kofinas, P. *J. Magn. Magn. Mater.* **2005**, *288*, 219–223.
(14) Costanzo, P. J.; Beyer, F. L. *Macromolecules* **2007**, *40* (11), 3996–4001.
(15) Jeng, U. S.; Sun, Y. S.; Lee, H. Y.; Hsu, C. H.; Liang, K. S.; Yeh, S. W.; Wei, K. H. *Macromolecules* **2004**, *37* (12), 4617–4622.
(16) Lin, Y.; Boker, A.; He, J. B.; Sill, K.; Xiang, H. Q.; Abetz, C.; Li, X. F.; Wang, J.; Emrick, T.; Long, S.; Wang, Q.; Balazs, A.; Russell, T. P. *Nature (London)* **2005**, *434* (7029), 55–59.
(17) Tadd, E. H.; Bradley, J.; Tannenbaum, R. *Langmuir* **2002**, *18* (6), 2378–2384.
(18) Weng, C. C.; Wei, K. H. *Chem. Mater.* **2003**, *15* (15), 2936–2941.
(19) Yeh, S. W.; Wu, T. L.; Wei, K. H. *Nanotechnology* **2005**, *16* (6), 683–687.
(20) Zhang, Q.; Xu, T.; Butterfield, D.; Misner, M. J.; Ryu, D. Y.; Emrick, T.; Russell, T. P. *Nano Lett.* **2005**, *5*, 357–361.
(21) Misner, M. J.; Skaff, H.; Emrick, T.; Russell, T. P. *Adv. Mater.* **2003**, *15*, 221–224.
(22) Darling, S. B.; Yufa, N. A.; Cisse, A. L.; Bader, S. D.; Sibener, S. J. *Adv. Mater.* **2005**, *17* (20), 2446–2450.
(23) Lauter-Pasyuk, V.; Lauter, H. J.; Gordeev, G. P.; Muller-Buschbaum, P.; Toperverg, B. P.; Jernenkov, M.; Petry, W. *Langmuir* **2003**, *19* (19), 7783–7788.
(24) Lauter-Pasyuk, V.; Lauter, H. J.; Gordeev, G. P.; Muller-Buschbaum, P.; Toperverg, B. P.; Petry, W.; Jernenkov, M.; Petrenko, V.; Aksenov, V. *Physica B* **2004**, *350*, 939–942.
(25) Park, M. J.; Char, K. *Langmuir* **2006**, *22* (4), 1375–1378.
(26) Park, M. J.; Park, J.; Hyeon, T.; Char, K. *J. Polym. Sci., Part B: Polym. Phys.* **2006**, *44* (24), 3571–3579.
(27) Bockstaller, M. R.; Lapetnikov, Y.; Margel, S.; Thomas, E. L. *J. Am. Chem. Soc.* **2003**, *125* (18), 5276–5277.
(28) Thompson, R. B.; Ginzburg, V. V.; Matsen, M. W.; Balazs, A. C. *Science* **2001**, *292* (5526), 2469–2472.
(29) Thompson, R. B.; Ginzburg, V. V.; Matsen, M. W.; Balazs, A. C. *Macromolecules* **2002**, *35* (3), 1060–1071.
(30) Bockstaller, M. R.; Thomas, E. L. *Phys. Rev. Lett.* **2004**, *93*, 166106.
(31) Chiu, J. J.; Kim, B. J.; Yi, G. R.; Bang, J.; Kramer, E. J.; Pine, D. J. *Macromolecules* **2007**, *40* (9), 3361–3365.
(32) Matsen, M. W.; Thompson, R. B. *Macromolecules* **2008**, *41* (5), 1853–1860.
(33) Chiu, J. J.; Kim, B. J.; Kramer, E. J.; Pine, D. J. *J. Am. Chem. Soc.* **2005**, *127* (14), 5036–5037.
(34) Kim, B. J.; Chiu, J. J.; Yi, G. R.; Pine, D. J.; Kramer, E. J. *Adv. Mater.* **2005**, *17* (21), 2618–2622.
(35) Kim, B. J.; Bang, J.; Hawker, C. J.; Kramer, E. J. *Macromolecules* **2006**, *39* (12), 4108–4114.
(36) Kim, B. J.; Fredrickson, G. H.; Hawker, C. J.; Kramer, E. J. *Langmuir* **2007**, *23* (14), 7804–7809.
(37) Listak, J.; Bockstaller, M. R. *Macromolecules* **2006**, *39* (17), 5820–5825.
(38) Deshmukh, R. D.; Buxton, G. A.; Clarke, N.; Composto, R. J. *Macromolecules* **2007**, *40* (17), 6316–6324.
(39) Sun, S. H.; Zeng, H. *J. Am. Chem. Soc.* **2002**, *124* (28), 8204–8205.
(40) Ohno, K.; Morinaga, T.; Koh, K.; Tsujii, Y.; Fukuda, T. *Macromolecules* **2005**, *38* (6), 2137–2142.

(41) Anastasiadis, S. H.; Russell, T. P.; Satija, S. K.; Majkrzak, C. F. *J. Chem. Phys.* **1990**, *92* (9), 5677–5691.
(42) Morkved, T. L.; Lopes, W. A.; Hahm, J.; Sibener, S. J.; Jaeger, H. M. *Polymer* **1998**, *39* (16), 3871–3875.
(43) Sivaniah, E.; Hayashi, Y.; Matsubara, S.; Kiyono, S.; Hashimoto, T.; Kukunaga, K.; Kramer, E. J.; Mates, T. *Macromolecules* **2005**, *38* (5), 1837–1849.
(44) Huang, E.; Mansky, P.; Russell, T. P.; Harrison, C.; Chaikin, P. M.; Register, R. A.; Hawker, C. J.; Mays, J. *Macromolecules* **2000**, *33* (1), 80–88.
(45) Duque, D.; Katsov, K.; Schick, M. *J. Chem. Phys.* **2002**, *117* (22), 10315–10320.
(46) Burgaz, E.; Gido, S. P. *Macromolecules* **2000**, *33* (23), 8739–8745.
(47) Stoykovich, M. P.; Muller, M.; Kim, S. O.; Solak, H. H.; Edwards, E. W.; de Pablo, J. J.; Nealey, P. F. *Science* **2005**, *308* (5727), 1442–1446.
(48) Chung, H.; Ohno, K.; Fukuda, T.; Composto, R. J. *Nano Lett.* **2005**, *5* (10), 1878–1882.
(49) Xu, C.; Ohno, K.; Ladmiral, V.; Composto, R. J. *Polymer* **2008**, *49*, 3568–3577.
(50) Field, M.; Smith, C. J.; Awschalom, D. D.; Mendelson, N. H.; Mayes, E. L.; Davis, S. A.; Mann, S. *Appl. Phys. Lett.* **1998**, *73* (12), 1739–1741.
(51) Si, S.; Kotal, A.; Mandal, T. K.; Giri, S.; Nakamura, H.; Kohara, T. *Chem. Mater.* **2004**, *16*, 3489–3496.
(52) Ozkaya, T.; Toprak, M. S.; Baykal, A.; Kavas, H.; Koseoglu, Y.; Aktas, B. *J. Alloys Compd.* **2008**, in press.
(53) Chitu, L.; Jergel, M.; Majkova, E.; Luby, S.; Capek, I.; Satka, A.; Ivan, J.; Kovac, J.; Timko, M. *Mater. Sci. Eng., C* **2007**, *27*, 1415–1417.
(54) Zeng, H.; Black, C. T.; Sandstrom, R. L.; Rice, P. M.; Murray, C. B.; Sun, S. *Phys. Rev. B* **2006**, *73*, 020402.
(55) Morrish, A. H. *The Physical Principles of Magnetism*; IEEE Press: New York, 2001.
(56) He, Y. P.; Wang, S. Q.; Li, C. R.; Miao, Y. M.; Wu, Z. Y.; Zou, B. S. *J. Phys. D: Appl. Phys.* **2005**, *38*, 1342–1350.
(57) Goya, G. F.; Berquo, T. S.; Fonseca, F. C.; Morales, M. P. *J. Appl. Phys.* **2003**, *94*, 3520–3528.
(58) Goya, G. F.; Fonseca, F. C.; Jardim, R. F.; Muccillo, R.; Carreno, N. L. V.; Longo, E.; Leite, E. R. *J. Appl. Phys.* **2003**, *93*, 6531–6533.
(59) Gamarra, L. F.; Brito, G. E. S.; Pontuschka, W. M.; Amaro, E.; Parma, A. H. C.; Goya, G. F. *J. Magn. Magn. Mater.* **2005**, *289*, 439–441.
(60) Kechrakos, D.; Trohidou, K. N. *Phys. Rev. B* **1998**, *58*, 12169–12177.
(61) Morup, S.; Bodker, F.; Hendriksen, P. V.; Linderoth, S. *Phys. Rev. B* **1995**, *52*, 287–294.
(62) Wang, R. F.; Nisoli, C.; Freitas, R. S.; Li, J.; McConville, W.; Cooley, B. J.; Lund, M. S.; Samarth, N.; Leighton, C.; Crespi, V. H.; Schiffer, P. *Nature (London)* **2006**, *439*, 303–306.

MA8022266